doi.org/10.36721/PJPS.2026.39.217.1

Effects of vitexin on angiotensin II-induced kidney injury and its relationship with the AT1R/Smad3 pathway

Yazhen Huang[1], Wenshuai Mao[2], Yalu Huang[3] and Hong Ge[1]*

[1]Department of Nephrology, Zhejiang Medical and Health Group Hangzhou Hospital, Hangzhou, Zhejiang, 310030, China
[2]Cardiovascular Surgery, ZheJiang Provincial People's Hospital, Hangzhou, Zhejiang, 310014, China
[3]Department of Respiratory, The Affiliated Hospital of Hangzhou Normal University, Hangzhou, Zhejiang, 310015, China

Abstract: **Background**: Angiotensin II (Ang II)-induced kidney injury is a critical pathway in the progression of chronic kidney disease, with the AT1R/Smad3 signaling axis playing a well-established role. The natural flavonoid vitexin has shown multi-organ protective effects, but its role and mechanism in Ang II-induced renal injury remain unclear. **Objectives**: To investigate the protective effect of vitexin against Ang II-induced kidney injury and explore whether its mechanism involves modulation of the AT1R/Smad3 pathway. **Methods**: *In-vitro*, Ang II-induced HK-2 cell injury models were treated with vitexin (20 μmol/L) or valsartan (1 μmol/L). Cell viability and SOD activity were assessed. Protein levels of AT1R, Smad2/3, p-Smad2/3, and Smad7 were detected by Western blotting. *In-vivo*, C57BL/6 mice with Ang II-induced kidney injury (1.1 mg/kg/d, 21 days) received vitexin (60 mg/kg, every other day) or vehicle. Blood pressure, urinary protein/creatinine ratio, renal histopathology (HE, PAS, Masson staining) and expression of AT1R/Smad3 pathway components were evaluated. **Results**: Vitexin significantly improved cell viability and SOD activity in HK-2 cells, comparable to valsartan. It downregulated AT1R, Smad2/3 and p-Smad2/3 while upregulating Smad7. In mice, vitexin lowered systolic blood pressure and the urinary protein/creatinine ratio, and alleviated renal histopathological damage, glomerular sclerosis, and fibrosis. It also reduced AT1R, p-Smad2/3, and CTGF expression and increased Smad7 in renal tissue. **Conclusion**: Vitexin attenuates Ang II-induced kidney injury by modulating the AT1R/Smad3 signaling pathway, suggesting its potential as a therapeutic candidate for renal injury. Further studies are needed to validate causal mechanisms and pharmacokinetics.

Keywords: Angiotensin II; AT1R; Kidney injury; Smad3; Vitexin

Submitted on 04-12-2025 – Revised on 07-02-2026 – Accepted on 26-02-2026

INTRODUCTION

Chronic kidney disease (CKD) is characterized by a persistent and progressive decline in key renal functions such as filtration and excretion, leading to irreversible injury. Previous studies have reported that with a prevalence as high as 13%, CKD represents a major cause of mortality and poses a significant threat to global public health (Wang *et al*., 2023, Ying *et al*., 2024). Previously, there have been reports, in renal injury pathogenesis, angiotensin II (Ang II), the core effector of the renin-angiotensin system (RAS), plays a pivotal role in driving renal damage and promoting its progression toward CKD (Xu *et al*., 2022). The RAS operates as a hormonal cascade, initiated by angiotensinogen (AGT) expression, followed by renin-mediated conversion to Ang I and subsequent cleavage to Ang II by angiotensin-converting enzyme (Ahmad *et al*., 2023). Previous studies have shown that ACE inhibitors (ACEIs) or angiotensin II receptor blockers (ARBs) can effectively delay the progression of confirmed chronic kidney disease (CKD), especially when accompanied by proteinuria (Zeng *et al*., 2025). These findings underscore the critical role of Ang II in CKD progression. Previous studies have shown that, ACEIs are associated with adverse effects such as dry cough and hypotension (Gregg *et al*., 2023), highlighting the need for alternative therapeutic strategies. Therefore, elucidating the molecular mechanisms underlying Ang II-induced renal injury and identifying novel therapeutic agents that can effectively intervene in this process are of significant importance for the treatment of CKD.

TGF-β1/Smad signaling is a key regulator of renal fibrosis. Previous studies have shown, in CKD, Ang II binding to AT1R significantly upregulates TGF-β1 and activates Smad2/3, thereby inducing the transcription of profibrotic miRNAs and lncRNAs, which collectively promote renal fibrosis (Chen *et al*., 2025; Feng *et al*., 2024; Dong *et al*., 2022). Numerous studies (Zhu *et al*., 2023; Wang *et al*., 2025) have confirmed that Smad3 phosphorylation is significantly elevated in various animal models of kidney injury, including diabetic nephropathy and CKD. Previously, there have been reports, blocking Smad3 activation with the inhibitor paroxetine significantly reduces collagen deposition and alleviates renal fibrosis in mice (Cheng *et al*., 2025). These findings suggest that the AT1R/Smad3 pathway is involved in Ang II-induced kidney injury. There have been reports vitexin is a natural flavonoid carbon glycoside widely found in various medicinal plants and possesses diverse pharmacological

**Corresponding author:* e-mail: mrn2025@163.com

activities, including anti-inflammatory, antioxidant, and anti-fibrotic effects (Liu *et al.*, 2025). Recent studies have shown that Vitexin exhibits organ-protective effects in multiple disease models. Previously, there have been reports, found that Vitexin can inhibit gastric cancer growth and metastasis through the HMGB1-mediated PI3K/AKT/mTOR/HIF-1α signaling pathway (Zhou P *et al*., 2022). Previously, there have been reports, Vitexin can alleviate cerebral ischemia-reperfusion injury in rats by inhibiting the TLR4/NF-κB pathway (Guo and Shi, 2023). In the context of fibrotic diseases, a previous study (Farooq *et al*., 2022) demonstrated that Vitexin reduces the expression of fibrotic markers, including collagen AI, TGF-β, and α-smooth muscle actin, in the liver tissues of Schistosoma mansoni-infected mice, thereby alleviating hepatic fibrosis. These findings suggest that Vitexin may exert its protective effects through multi-target mechanisms.

However, whether vitexin can mitigate Ang II-induced renal injury, particularly through modulation of the AT1R/Smad3 pathway, remains unknown. Although vitexin has demonstrated renoprotective effects in cisplatin-induced injury models, its role and mechanisms in Ang II-dependent renal injury remain unexplored. Therefore, this study aims to explore the effects of Vitexin on Ang II-induced renal injury and its relationship with the AT1R/Smad3 pathway, to provide new therapeutic strategies for Ang II-related renal injury.

MATERIALS AND METHODS

Experimental materials and instruments
See Tables 1-1 and 1-2.

Experimental methods
Experimental cells
Human proximal renal tubular epithelial cells (HK-2) were purchased from Yansheng Industrial (Shanghai).

Experimental drugs
Vitexin Solution Preparation: Based on preliminary experiments and the dosage range reported in previous literature (Maji *et al*., 2021), based on preliminary experiments and prior literature, this study selected concentrations that demonstrated significant protective effects and low toxicity. Vitexin standard (purity > 98%, Beijing Kang Ruina Biotechnology) was weighed and dissolved in dimethyl sulfoxide (DMSO) to prepare a 20 mmol/L stock solution, which was stored at -20°C. Before use, the stock solution was diluted with serum-free DMEM/F12 medium to a final concentration of 20 μmol/L. In all *in-vitro* experiments, the final DMSO concentration was maintained at 0.1% (v/v). Model and control groups received an equal volume of 0.1% DMSO to control for solvent effects.
Valsartan solution preparation: Valsartan capsules (manufacturer: Beijing Novartis Pharmaceutical Co., Ltd., specification: 80 mg, batch number: H20040217) were ground and dissolved in DMSO to prepare a 10 mmol/L stock solution, which was then diluted to a final concentration of 1 μmol/L for *in-vitro* experiments (Nasr *et al*., 2022).

In-vivo administration solution: For *in-vivo* experiments, Vitexin was administered at a dose of 60 mg/kg. This dose was determined based on preliminary experiments and previous studies from our laboratory in similar fibrosis models. The final DMSO concentration was 10% (v/v) to ensure solubility while minimizing solvent toxicity. The positive control group received Valsartan at a dose of 10 mg/kg/day, administered via drinking water (Jiang *et al*., 2017). Mice in the model and normal control groups were injected intraperitoneally with an equal volume of physiological saline containing 10% DMSO to control for solvent effects.

Cell culture
HK-2 cells were routinely cultured in a 37°C, 5% CO_2 incubator using DMEM/F12 medium containing 10% fetal bovine serum and 1% penicillin-streptomycin.

Cell grouping and intervention
To establish an Ang II-induced cellular injury model, HK-2 cells were serum-starved in serum-free medium for 12 hours and then randomly divided into four groups: Control group: cultured normally with only 0.1% DMSO added. Model group: treated with Ang II (1 μmol/L) and 0.1% DMSO (Zhao *et al*., 2023). Valsartan group: treated simultaneously with Ang II (1 μmol/L) and Valsartan (1 μmol/L). Vitexin group: treated simultaneously with Ang II (1 μmol/L) and Vitexin (20 μmol/L). All groups were treated for 24 hours. After treatment, cells were collected for subsequent experiments.

Construction of a mouse model of kidney injury induced by Ang II
All animal experimental protocols in this study were approved by the Ethics Committee of Zhejiang Medical and Health Group Hangzhou Hospital (Approval No.: SCXK(Zhe)2025-1201) and strictly adhered to international guidelines for the care of laboratory animals and the ARRIVE guidelines.

(1) Preparation of Ang II solution: Based on a dosage of 1.1 $mg \cdot kg^{-1} \cdot day^{-1}$ per mouse for 21 days, each osmotic pump was filled with 200 μL of solution containing 0.5775 mg Ang II.
(2) Pretreatment and perfusion of osmotic pump: Under aseptic conditions, Ang II solution was slowly injected into the osmotic pump using a 0.5 μL microsyringe, and the infusion catheter was connected. After assembly, the pump was pretreated in sterile saline at 37°C for 24 h to activate the continuous release function.
(3) Pump implantation: C57BL/6 mice (male, 8 weeks old, weighing 20-25 g) were anesthetized via intraperitoneal

Table 1-1: Main reagents.

Name	Company
DMEM/F12 Culture Medium	Corning Incorporated (USA)
Fetal Bovine Serum	Lanzhou Bailing Biotechnology Co., Ltd.
Angiotensin II	MedChemExpress (USA)
Phosphate Buffered Sodium (PBS)	Shanghai Sangon Biotech Co., Ltd.
0.25% Trypsin	Gibco (USA)
75% Ethanol	Shanghai Maclean Biotechnology Co., Ltd.
Cell Cryopreservation Medium	Shanghai Yisheng Biotechnology Co., Ltd.
Traditional Chinese Medicine Pieces	China Resources Sanjiu Pharmaceutical Co., Ltd.
Captopril Standard	China National Institutes for Food and Drug Control
CCK-8 Detection Kit	Dojindo (Japan)
RIPA Lysis Buffer	Shanghai Beyotime Biotechnology Co., Ltd.
BCA Protein Assay Kit	Nanjing Novizan Biotechnology Co., Ltd.
Separating Gel Preparation Buffer	Shanghai Yamei Biotechnology Co., Ltd.
Temed Tetramethylethylenediamine	Beijing Solarbio Technology Co., Ltd.
Electrotransfer and Electrophoresis Buffer	Bio-Rad Laboratories (USA)
Methanol	Shanghai Maclean Biotechnology Co., Ltd.
Blocking Skim Milk Powder	BD Biotech (USA)
5× Blocking-Wash Buffer	Beijing Zhongshan Jinqiao Biotechnology Co., Ltd.
Rainbow prestained protein molecular weight standard (MARKER)	Thermo Scientific (USA)
TLR4 Antibody, NF-κB Antibody, and β-actin Antibody	Santa Cruz Biotechnology Co., Ltd. (USA)
AT1R Antibody and AT2R Antibody	Santa Cruz Biotechnology Co., Ltd. (USA)
Smad2/3 Antibody, p-Smad2/3 Antibody, and Smad7 Antibody	Cell Signaling Technology Co., Ltd. (USA)
CTGF Antibody	Abcam Co., Ltd. (USA)
Goat Anti-Rabbit IgG and Goat Anti-Mouse IgG Secondary Antibodies	Beijing Zhongshan Jinqiao Biotechnology Co., Ltd.
ECL PI High-Sensitive Chemiluminescent Substrate Solution	Shanghai Tianneng Technology Co., Ltd.

Note: All primary antibodies have been verified and can detect a single specific band of the expected size in Western Blot.

Table 1-2: Main instruments

Item	Company
LX-200 Mini Centrifuge	Hunan Xiangyi Laboratory Instrument Development Co., Ltd.
Cell Culture CO_2 Incubator and Clean Bench	Thermo Fisher Scientific (USA)
DNP-9082 Electric Thermostatic Incubator	Shanghai Yiheng Scientific Instruments Co., Ltd.
ELx800 Fully Automated Microplate Reader	Thermo Fisher Scientific (USA)
VORTEXGENIUS3 Vortex Shaker	Dalong Xingchuang Experimental Instruments Co., Ltd.
ENDURO Electrophoresis System	Bio-Rad (USA)
TS-200 Dual-Layer Digital Display Decolorization Shaker	Shanghai Xiren Scientific Instruments Co., Ltd.
ChemiDoc XRS+ Chemiluminescence Imaging System	Shanghai Tianneng Technology Co., Ltd.
Cryostat and Fluorescence Microscope System	Leica (Germany)
3-30K High-Speed Low-Temperature Centrifuge	Eppendorf (Germany)

Table 2: PCR primer sequences.

Gene	Sequences	Product length
GAPDH	Forward primer:5'-CTGGAGAAACCTGCCAAGTATG-3’ Reverse primer:5'-GGTGGAAGAATGGGACTTGCT-3’	138
AngII	Forward primer:5'-CCACGCACAGCACCCTATTT-3' Reverse primer:5’-GCCCCTTCTTTATCCAACTCAG-3’	306
AT1R	Forward primer:5'-CACTCCTCTACTTATGTAGCAG-3’ Reverse primer:5'-AGATGTACCTAGTATGTCACGTT-3’	85
SMAD4	Forward primer:5'-CTCATGTGATCTATGCCCGTC-3’ Reverse primer:5'--AGGTGATACAACTCGTTCGTAGT-3’	22

injection of 5% chloral hydrate (0.4 mL/100 g). The skin in the scapular region was shaved and disinfected and a longitudinal incision approximately 2 cm in length was made along the spine, followed by blunt dissection of subcutaneous tissue. A pretreated osmotic pump (release rate 0.25 μL/h) was subcutaneously implanted with the catheter opening facing inward. Post-surgery, the wound was closed in layers. All surgical procedures were performed under aseptic conditions. For three consecutive days after surgery, mice were administered analgesics and closely monitored for body weight, activity levels and wound healing. Mice in both the model and treatment groups were subcutaneously implanted with an Ang II osmotic pump.

Animal grouping and intervention

To achieve 80% statistical power (power=0.8) and to detect the expected effect size (determined from preliminary experiments and literature), we included 6 mice per group (n=6). A total of 24 C57BL/6 mice were randomly assigned to four groups: Normal control group (n=6): Only implanted with an empty pump (without Ang II) and received intraperitoneal injections of 10% DMSO in saline every other day. Model group (n=6): Implanted with an Ang II pump and received intraperitoneal injections of 10% DMSO in saline every other day. Vitexin group (n=6): Implanted with an Ang II pump and received intraperitoneal injections of Vitexin (60 mg/kg, dissolved in 10% DMSO in saline) every other day. Valsartan group (n=6, positive control group): Implanted with an Ang II pump and treated with Valsartan (approximately 10 mg/kg/day) administered via drinking water. All interventions lasted for 21 days. Humane endpoint criteria were defined as: weight loss exceeding 20% of baseline body weight, severe mobility impairment, inability to eat or drink, or other signs of significant distress. No animals met these criteria during the experiment. After the intervention period, urine and kidney tissue samples were collected from each group of mice.

Assessment of cellular experimental parameters

Cell viability and SOD activity assays

Cell viability was assessed using the CCK-8 assay (Chen *et al*., 2022). After treatment as described in Section 2.2.4, the original medium was removed from HK-2 cells in all groups. CCK-8 working solution, diluted in fresh complete medium (CCK-8 reagent: medium = 1:10), was added to each well. The plates were incubated in a 37°C, 5% CO_2 incubator for 2 hours in the dark. Following incubation, the optical density (OD) at 450 nm was measured for each well using a microplate reader (Thermo Fisher Scientific, USA). Cell viability was calculated using the formula: Cell viability (%) = [(OD_treated - OD_blank) / (OD_control - OD_blank)] × 100%. Each group was assayed in 6 replicate wells (n=6), and the experiment was independently repeated 3 times. SOD activity was measured using a WST-8-based SOD assay kit (Cao *et al*., 2022). After treatment, the culture medium was discarded and the cells were gently washed twice with ice-cold PBS. An appropriate volume (100 μL) of cell lysis buffer (containing protease inhibitors) was added to each well and cells were lysed on ice for 30 minutes. Cell lysates were collected using a cell scraper, centrifuged at 12,000 rpm for 15 minutes at 4°C and the supernatant was collected as the sample for assay. The procedure followed the manufacturer's instructions for the SOD activity assay kit (Dojindo, Japan): the sample, WST-8 working solution and enzyme reaction initiator were sequentially added to a 96-well plate. After thorough mixing, the plate was incubated at 37°C in the dark for 30 minutes. The OD at 450 nm was measured using a microplate reader. The SOD inhibition rate was calculated according to the formula provided by the kit: The SOD inhibition rate (%) was calculated using the following formula: SOD inhibition rate (%) = [(OD($blank_1$) - OD($blank_2$) - OD(sample) - OD($blank_2$))] / OD($blank_1$) - OD($blank_2$) × 100%. where $blank_1$ is the reaction system without the sample, and $blank_2$ is the reaction system without the sample but containing the SOD inhibitor. Each group was assayed with 6 biological replicates (n=6) and the experiment was independently repeated three times.

Western Blotting Analysis

Total cellular protein was extracted using RIPA lysis buffer (containing protease and phosphatase inhibitors), and protein concentration was determined using the BCA method (Löptien *et al*., 2024). Equal amounts of protein (30 μg) were separated by 10% SDS-PAGE electrophoresis and then transferred to a PVDF membrane using the wet transfer method. After transfer, the membrane was blocked with 5% skim milk at room temperature for 2 hours, followed by incubation with the corresponding primary antibodies at 4°C overnight. The primary antibodies used and their dilution ratios were as follows: AT1R (1:1000), AT2R (1:1000), Smad2/3 (1:1000), p-Smad2/3 (1:1000), Smad7 (1:1000), CTGF (1:800) and the internal reference β-actin (1:5000). The next day, the membrane was washed three times with TBST, incubated with the corresponding horseradish peroxidase-labeled secondary antibody (1:5000) at room temperature for 1 hour and then washed with TBST. Protein bands were visualized using ECL chemiluminescence reagent and imaged with a chemiluminescence imaging system (ChemiDoc XRS+, Shanghai Tianneng Technology Co., Ltd.). The gray values of the target bands were quantified using ImageJ (National Institutes of Health, USA). The expression levels of each protein were normalized to β-actin. Detection of each protein index was based on at least three independent cell experiments.

Animal experiment indicator detection

Measurement of Systolic Blood Pressure, Urinary Protein, and Creatinine

I. *SBP Detection*: Before the formal experiment, all C57BL/6 mice underwent a 5-day acclimatization training

period for tail artery blood pressure measurement. The blood pressure measurement system was pre-activated and the ambient temperature was maintained at approximately 25°C. Mice were placed in a specially designed fixation device, and their tails were kept in a constant-temperature heater at 37°C for 10 minutes to promote full vasodilation. Heart rate curves were monitored simultaneously and SBP values were recorded once the heart rate stabilized. Five measurements were repeated for each individual, with an interval of at least 2 minutes between adjacent measurements. II. *Urine Protein Detection*: Urine samples were collected immediately after euthanasia via bladder puncture. All assays were performed according to the manufacturer's instructions: (1) Blank tubes, standard tubes and test tubes were prepared. 50 μL of ultrapure water, protein standard, or urine sample were added to each tube.

(2) 3.0 mL of CBB working solution was precisely added to each reaction tube and thoroughly mixed. (3) 200 μL of the mixture was placed in a 96-well plate and reacted for 5 minutes. (4) The absorbance was measured at 595 nm. (5) Sample concentration was calculated and expressed in mg/L. III. *Urine Creatinine Detection*: After euthanizing C57BL/6 mice, urine samples were immediately collected by bladder puncture and stored in a low-temperature environment for testing. The detection process strictly followed the kit operation specifications: (1) Set up blank wells, standard wells and test wells and add 6 μL of triple-distilled water or standard in sequence. (2) Add 180 μL of enzyme reaction solution A (reagent one) to each well, incubate for 5 min and immediately measure the initial absorbance A1 at a wavelength of 546 nm. (3) Continue to add 60 μL of enzyme reaction solution B (reagent two) to each well, incubate again for 5 min and read the absorbance value A2 at the same wavelength. (4) Calculate the creatinine content in the urine sample according to the standard curve and the difference between the two absorbance values and express the results in mmol/L.
Note: The urine protein/creatinine ratio (UACR) is used to assess renal function.

Histological Staining (HE, PAS, and Masson Trichrome)
Paraffin-embedded kidney tissue sections (4 μm) were deparaffinized and rehydrated, followed by staining with Hematoxylin and Eosin (HE), Periodic Acid-Schiff (PAS) and Masson's trichrome.

Renal Injury Score (HE staining): A semi-quantitative scoring method was employed, with two independent researchers blinded to the group assignments performing the assessments (Gisch *et al*., 2024). The scoring criteria were as follows: 0 points, no lesions; 1 point, lesion area <25%; 2 points, lesion area 25-50%; 3 points, lesion area 50-75%; 4 points, lesion area >75%. Parameters assessed included tubular dilation, vacuolar degeneration of epithelial cells, epithelial detachment, and cast formation.
Glomerulosclerosis Index (PAS staining): For each sample, at least 20 glomeruli were randomly selected, and the percentage of glomeruli exhibiting segmental or global sclerosis (characterized by increased mesangial matrix and capillary loop occlusion) was calculated.

Renal Interstitial Fibrosis Area (Masson staining): For each section, at least five non-overlapping fields of view were randomly selected under 200× magnification. The area of blue-stained collagen fibers as a percentage of the total renal cortical area was calculated using Image-Pro Plus 6.0 software.

AT1R immunohistochemical staining
After fixation, embedding and sectioning, kidney tissue underwent antigen retrieval and BSA blocking. It was incubated sequentially with primary antibody, secondary antibody and SABC reagent, followed by DAB staining, counterstaining and mounting (Rojansky *et al*., 2022). Observations under a microscope revealed brown-yellow staining as a positive result. The average optical density (AOD) was measured from 5 randomly selected fields of view using Image-Pro Plus 6.0.

mRNA expression detection (real-time quantitative PCR)
Total RNA was extracted from kidney tissue using the TRIzol method and reverse-transcribed into cDNA. Real-time quantitative PCR (qRT-PCR) was performed using the SYBR Green method on an ABI 7500 system (McKenney *et al*., 2024). Primer sequences are listed in table 2 of the original manuscript. The expression levels, such as Connective Tissue Growth Factor (CTGF), were calculated using the 2^-ΔΔCt method (Livak and Schmittgen, 2001), with GAPDH as the internal reference. Detection for each group included 6 independent biological samples, with each sample assayed in triplicate (three technical replicates).

Study scope, bias control and handling of confounding variables
This preliminary preclinical study aimed to explore the protective effects of Vitexin against Ang II-induced renal injury and its association with the AT1R/Smad3 pathway at the cellular and animal levels. The scope of work focused on pharmacodynamic evaluation and mechanistic correlation analysis and did not involve compound structural modification, systemic pharmacokinetics, long-term toxicity, or clinical translation research.

To control for research bias, the following measures were implemented: (1) *Randomization*: Groups were randomized using computer-generated random number tables after cell seeding and upon animal enrollment to ensure baseline comparability between groups. (2) *Blinded Assessment*: Histopathological scoring and quantitative analysis of Western blot band grayscale values were performed independently by two researchers blinded to group assignments and the results were averaged.

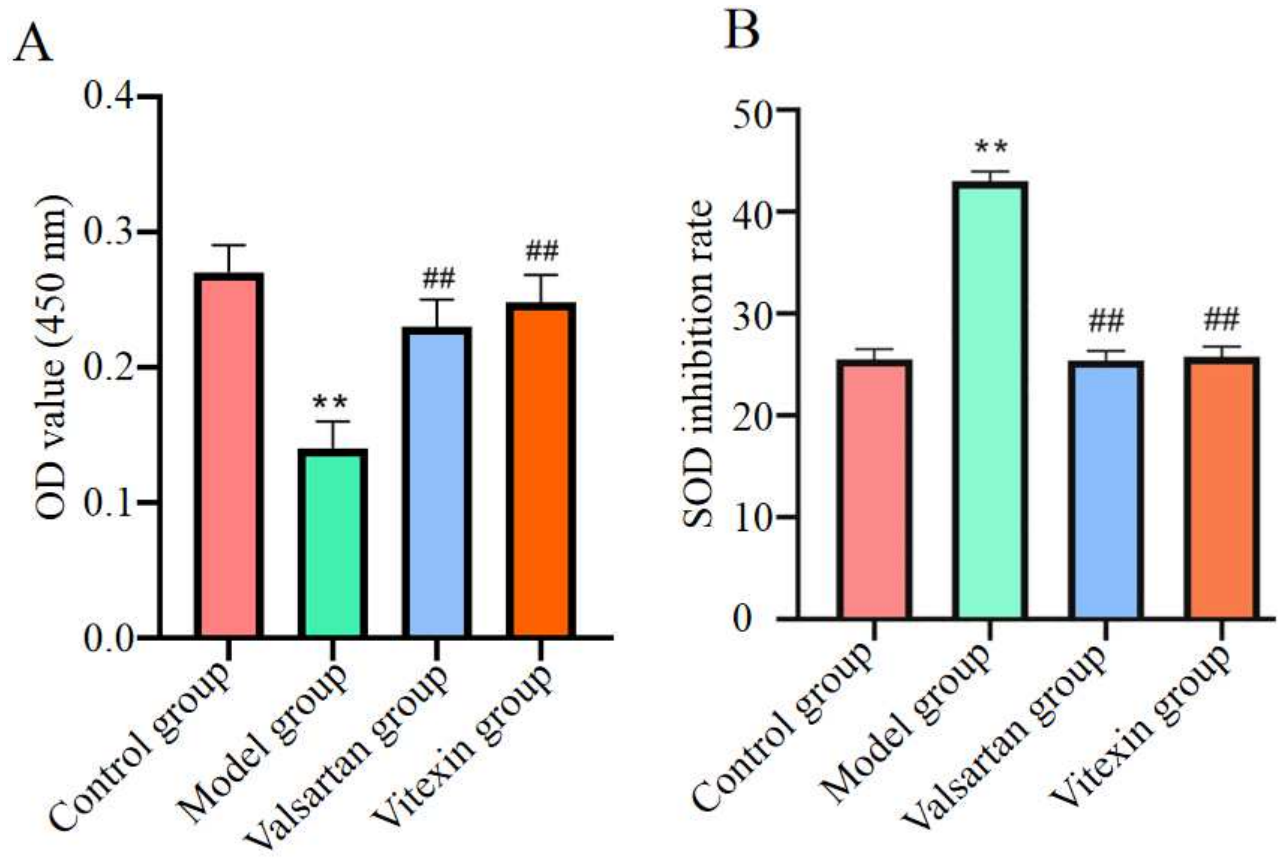

Fig. 1: The effect of Vitexin on the viability and SOD activity of HK-2 cells induced by Ang II
(A): Cell viability was detected by the CCK-8 method; (B): The SOD inhibition rate was detected by the WST-8 method. Data are expressed as mean ± SD (n=6). Compared with the control group, **P<0.01; compared with the model group, ##P<0.01

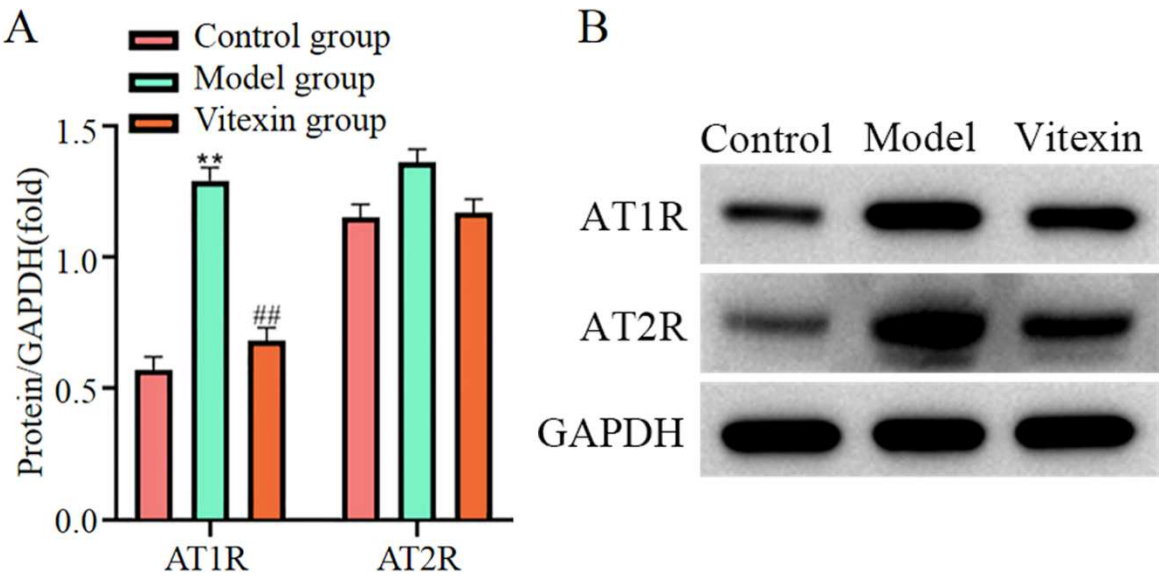

Fig. 2: Effects of vitexin on AT1R and AT2R expression in Ang II-induced kidney injury cells.
(A): AT1R and AT2R protein expression levels in each group; (B): AT1R and AT2R protein band diagram. Compared with the control group, **P<0.01; compared with the model group, ##P<0.01

(3) *Standardized Procedures and Data Analysis*: All assays were conducted strictly according to standard operating procedures. Clear inclusion and exclusion criteria were established (e.g., cell passage number, animal weight range), and data were processed according to a predefined statistical analysis plan to avoid selective outcome reporting.

To address potential confounding variables, the following were identified and controlled: (1) *Solvent effects*: All drug-treated groups and their corresponding model groups used the same final concentration of DMSO solvent (0.1% *in-vitro*, 10% *in-vivo*) to exclude the solvent's own effects on cell viability, animal physiological status and assay indicators. (2) *Individual animal differences*: C57BL/6 male mice of consistent age, weight and genetic background were selected and experiments were conducted in the same housing environment to minimize variation due to age, sex, genetics and environmental factors. (3) *Model stability*: The optimal Ang II induction concentration and duration were determined through preliminary experiments. Concurrent normal control and model control groups were established in the formal experiment to monitor model stability and systemic bias during the experimental process. (4) *Assay technical variation*: All biochemical and molecular biology assays included replicate wells/repeat samples and used reagents from the same batch. Target protein/mRNA levels were normalized to β-actin/GAPDH as internal references to minimize the impact of technical errors and loading variations.

Statistical analysis

We analyzed the data using SPSS 27.0 and GraphPad Prism 8.02. Normality was assessed using the Shapiro-Wilk test and homogeneity of variance was evaluated with Levene's test. Data are presented as mean ± SD. Comparisons between two groups were performed using unpaired t-tests, and multiple-group comparisons were conducted using one-way ANOVA followed by Tukey's post hoc test. Non-parametric tests were used when assumptions were not met. A P-value < 0.05 was considered statistically significant.

RESULTS

Vitexin improves Ang II-induced HK-2 cell viability and enhances antioxidant capacity

Compared with the control group, Ang II treatment significantly reduced HK-2 cell viability ($P<0.01$). Vitexin intervention significantly reversed the Ang II-induced decrease in cell viability ($P<0.01$) and its protective effect was comparable to that of the positive control drug, Valsartan (1 μmol/L) (Fig. 1A). Consistent with the cell viability results, Ang II treatment significantly inhibited SOD activity in HK-2 cells ($P<0.01$). Vitexin treatment significantly decreased the SOD inhibition rate ($P<0.01$) and its effect was similar to that of the Valsartan group (Fig. 1B).

Vitexin can reduce AT1R expression in Ang II-induced HK-2 cells, but does not affect AT2R expression

Western blot results (Fig. 2A, Fig. 2B) showed significantly increased AT1R level in model group ($P<0.01$), while decreased AT2R level without a difference ($P>0.05$); compared with model group, AT1R protein level in vitexin group was decreased ($P<0.01$), while AT2R level decreased. This indicates that vitexin can reduce AT1R expression in Ang II-induced HK-2 cells, but does not affect AT2R expression.

Effects of vitexin on the expression of smads pathway-related proteins in Ang II-induced kidney injury cells

Western Blot results (Fig. 3A) showed significantly increased expression of Smad2/3 and p-Smad2/3 in the model group, while decreased Smad7 expression ($\#P<0.05$); expression of Smad2/3 and p-Smad2/3 was significantly decreased in the vitexin group (Figs. 3C and 3D), while Smad7 expression showed an increasing trend (Fig. 3B), $P<0.05$. This implies that vitexin can effectively inhibit the over activation of the TGF-β/Smads signaling by blocking Smad2/3 phosphorylation and promoting Smad7 expression.

Vitexin reduces systolic blood pressure and urinary protein/creatinine ratio in Ang II-induced renal injury mice

SBP level (Fig. 4A) and urine protein/creatinine ratio (Fig. 4B) in the model group were significantly increased ($P<0.05$), whereas vitexin treatment decreased them ($P<0.05$), suggesting that vitexin effectively controls blood pressure in hypertensive mice and improves renal function indicators.

Vitexin significantly reduced the histopathological damage of renal tissue in mice with Ang II-induced renal injury

Results showed that, using HE staining to observe changes in renal damage in each group of mice (Figs. 5A and 5B), the glomeruli in the normal group showed intact structural morphology, with unobstructed capillary lumen; the model group showed significant shrinkage and the renal tubular epithelial cells showed pathological manifestations such as swelling and shedding, with a significantly higher renal damage score ($P<0.01$); the pathological changes in treatment group were alleviated with reduced renal damage score ($P<0.01$). PAS staining (Fig. 5C and 5D) showed intact glomerular structure and clearly defined components in normal group, but an increase in red-stained areas, glomerular deposition and marked thickening of the renal basement membrane, with a significantly larger glomerular sclerosis area in the model group ($P<0.01$), which were all reversed after treatment. Masson staining (Figs. 5E and 5F) showed increased blue-positive area in the renal interstitium and glomerular fibrosis in the model group ($P<0.01$), which were reduced in the treatment group ($P<0.01$). This indicates that vitexin treatment significantly reduced renal tissue damage, glomerular sclerosis and renal

interstitial fibrosis in mice, effectively inhibited collagen deposition and protected renal structure.

Vitexin down-regulates the expression of AT1R in the renal tissues of mice with Ang II-induced renal injury

A small amount of AT1R was observed in normal group, with a sparse distribution (Fig. 6); AT1R expression was significantly enhanced in model group and reduced in the treatment group. This indicates that vitexin can effectively inhibit AngII-induced upregulation of AT1R expression.

The effect of Vitexin on the expression of AT1R, SMADs-related proteins and mRNA in renal tissues of mice with Ang II-induced renal injury

Results (Figs. 7A, 7B, 7C, 7D and 7E) revealed significantly upregulated AT1R and p-Smad2/3 in kidneys of AngII-induced model mice but downregulated Smad7. After vitexin intervention, levels of AT1R and p-Smad2/3 were reduced but Smad7 increased. Smad2 level remained relatively stable across all groups. qRT-PCR analysis (Figs. 7F, 7G and 7H) showed significantly increased mRNA levels of AT1R, CTGF and Smad2 in model group, indicating that vitexin intervention effectively inhibited the excessive transcription of these genes. This suggests that vitexin mediates the AT1R/Smad3 signaling pathway by inhibiting CTGF, thus improving AngII-induced kidney injury.

DISCUSSION

Chronic kidney disease (CKD) is characterized by irreversible renal damage resulting from a persistent decline in the glomerular filtration rate and progressive loss of key physiological functions, including protein reabsorption and excretion. It has become a significant global public health burden. There have been reports in the pathological progression of CKD, angiotensin II (Ang II), a core effector molecule of the renin-angiotensin system (RAS), activates multiple pro-fibrotic and oxidative stress pathways—particularly the TGF-β/Smad signaling pathway—through its AT1R receptor. This mechanism is considered a key driver in the transition from renal injury to fibrosis (Rajabi *et al*., 2024). Therefore, identifying drugs that can effectively modulate the Ang II/AT1R axis and alleviate renal fibrosis is of significant value for CKD treatment. Previous studies have shown Vitexin is a natural flavonoid carbon glycoside with various pharmacological activities, including antioxidant, anti-inflammatory and anti-fibrotic effects (Liu *et al*., 2025). In recent years, multiple studies have reported the protective effects of vitexin in different organ injury models (Chen *et al*., 2025; Noor *et al*., 2022). However, its role and mechanisms in Ang II-induced kidney injury remain unclear. This study is the first to systematically evaluate the protective effects of vitexin and its regulatory role in the AT1R/Smad3 pathway using both Ang II-induced HK-2 cell and C57BL/6 mouse kidney injury models.

The research results demonstrate that Vitexin treatment significantly ameliorated the Ang II-induced decrease in HK-2 cell viability and enhanced intracellular superoxide dismutase (SOD) activity, with effects comparable to those of the first-line clinical drug Valsartan. In the animal model, Vitexin intervention significantly reduced systolic blood pressure and the urinary protein/creatinine ratio in Ang II-induced hypertensive mice and alleviated the extent of renal histopathological injury, glomerulosclerosis and interstitial fibrosis.

At the mechanistic level, this study focused on exploring the regulatory effect of vitexin on the AT1R/Smad3 pathway. In the progression of Ang II-induced renal injury, the AT1R/Smad3 signaling pathway has been identified by multiple studies as a key mechanism promoting renal fibrosis (Wu *et al*., 2022; Ye *et al*., 2023). Both in cellular and animal models, this study observed that Ang II stimulation significantly up-regulated the expression of AT1R and phosphorylated Smad2/3 (p-Smad2/3), accompanied by an increase in the fibrosis marker CTGF. These findings are consistent with the established role of this pathway in renal fibrosis.

Importantly, this study found that vitexin intervention significantly suppressed AT1R and p-Smad2/3 expression, pharmacologically validating the regulatory capacity of this natural compound on this pathway and providing mechanistic insights into its protective role in Ang II-associated renal injury. Further analysis revealed that while inhibiting p-Smad2/3, vitexin also up-regulated the expression of the negative regulator Smad7. Previously, there have been reports as an endogenous inhibitory protein of the TGF-β/Smad signaling pathway, Smad7 can block the phosphorylation and nuclear translocation of Smad2/3, thereby inhibiting the transcription of downstream fibrotic genes (Su *et al*., 2024).

The results of this study suggest that vitexin may restore Smad7 expression, rebalancing the Smad signaling pathway and alleviating excessive activation of pro-fibrotic signals induced by Ang II. This finding provides a new perspective on the intracellular mechanisms underlying vitexin's anti-fibrotic effects in the kidney. Furthermore, this study found that vitexin significantly reduced CTGF expression in renal tissue. Previous studies have shown CTGF is a key downstream effector of the TGF-β/Smad pathway, directly involved in the synthesis and deposition of extracellular matrix and serves as a core mediator in the progression of renal fibrosis (Livingston *et al*., 2023). The inhibition of CTGF expression by vitexin is highly consistent with histological improvements observed in Masson staining, including reduced collagen deposition, decreased glomerulosclerosis, and diminished interstitial fibrosis area. This indicates that vitexin may inhibit the fibrotic process at multiple stages by modulating the AT1R/Smad3/CTGF axis.

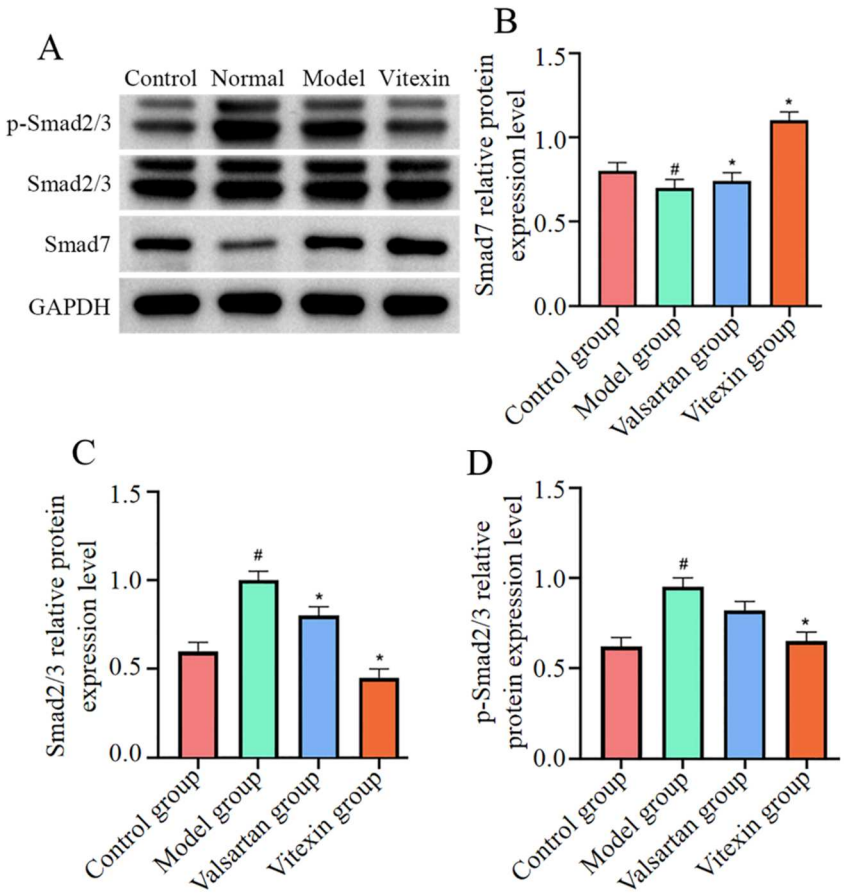

Fig. 3: Effects of vitexin on the expression of Smads pathway-related proteins in Ang II-induced renal injury cells.
(A): Bands of Smads pathway-related proteins; (B): Relative protein expression level of Smad7; (C): Relative protein expression level of Smad2/3; (D): Relative protein expression of p-Smad2/3. Compared with the control group, #P<0.05; compared with the model group, *P<0.05. Data are expressed as mean ± SD (n=6).

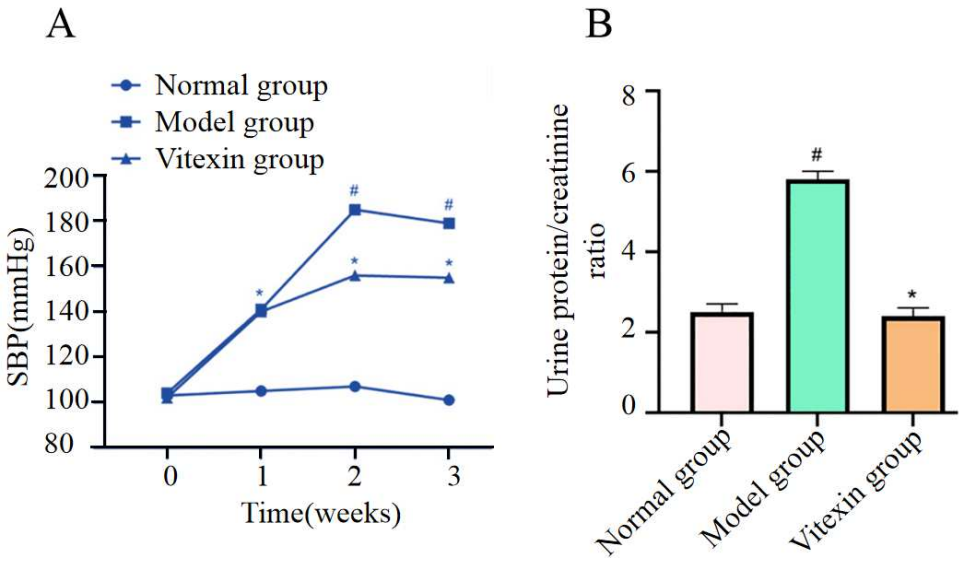

Fig. 4: Purple vitexin significantly reduced the SBP and urine protein/creatinine ratio in mice with Ang II-induced kidney injury.
(A): SBP levels in each group; (B): Urine protein/creatinine ratio levels. Compared with the normal group, #P<0.05; compared with the model group, *P<0.05. Data are expressed as mean ± SD (n=6).

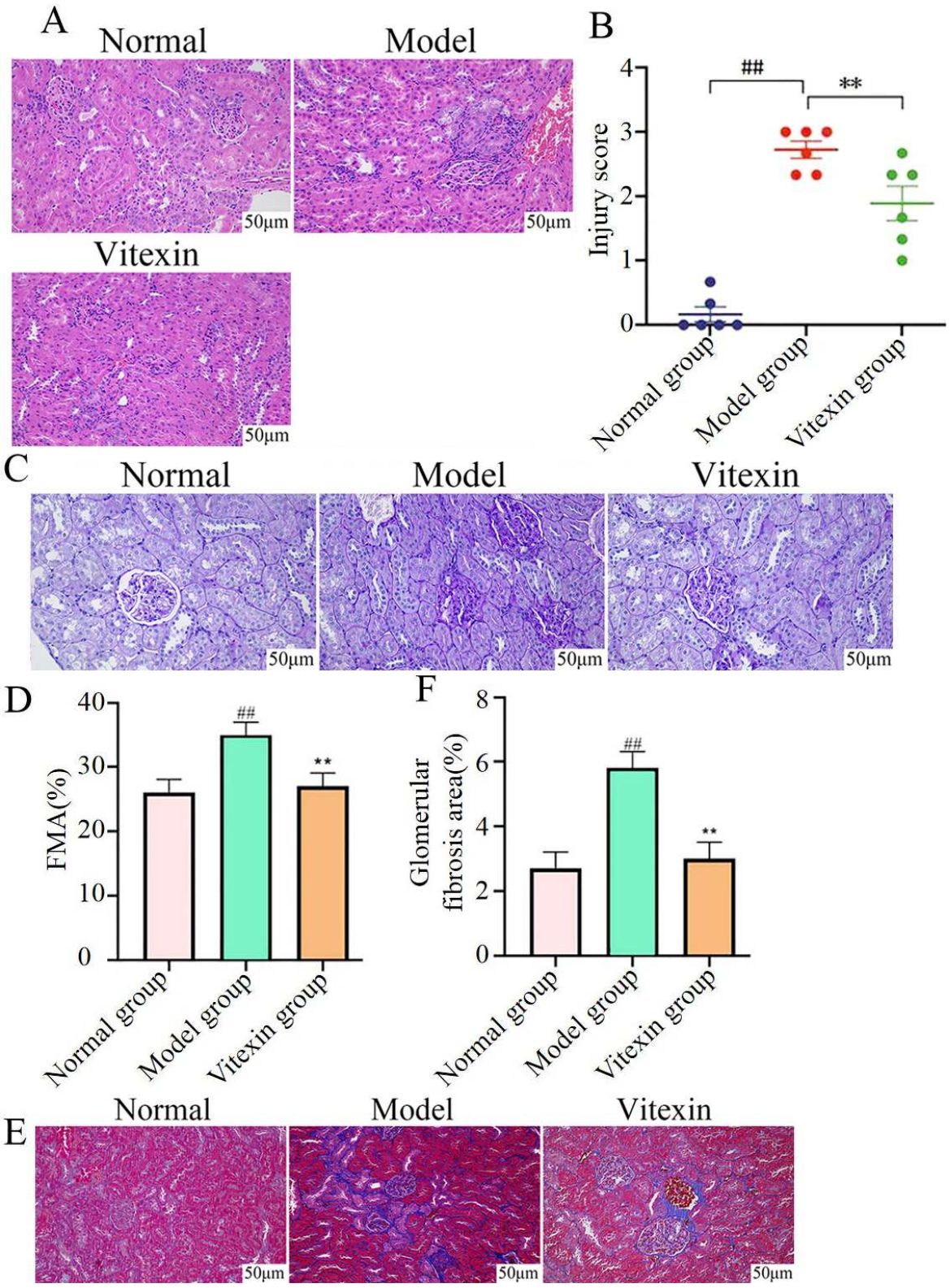

Fig. 5: Vitexin significantly reduced the histopathological damage of renal tissue in mice with Ang II-induced renal injury. (A): HE staining × 400 magnification; scale bar = 20 μm; (B): Damage score; (C): PAS staining × 400 magnification; scale bar = 20 μm; (D): Glomerular sclerosis area in each group; (E): Masson staining × 400 magnification; scale bar = 20 μm; (F): Glomerular fibrosis area in each group. Compared with the normal group, ##P < 0.01; compared with the model group, **P < 0.01. Data are expressed as mean ± SD (n=6).

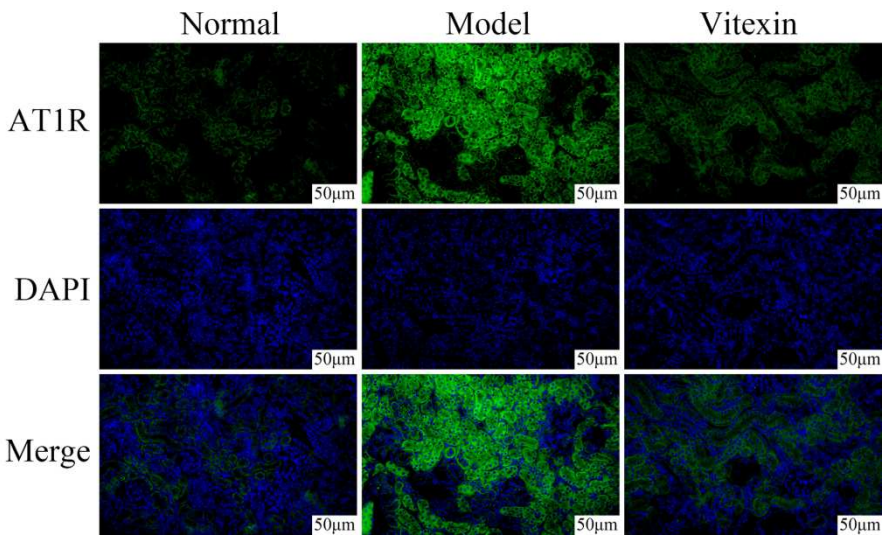

Fig. 6: Vitexin down-regulates the expression of AT1R in the renal tissues of mice with Ang II-induced renal injury.

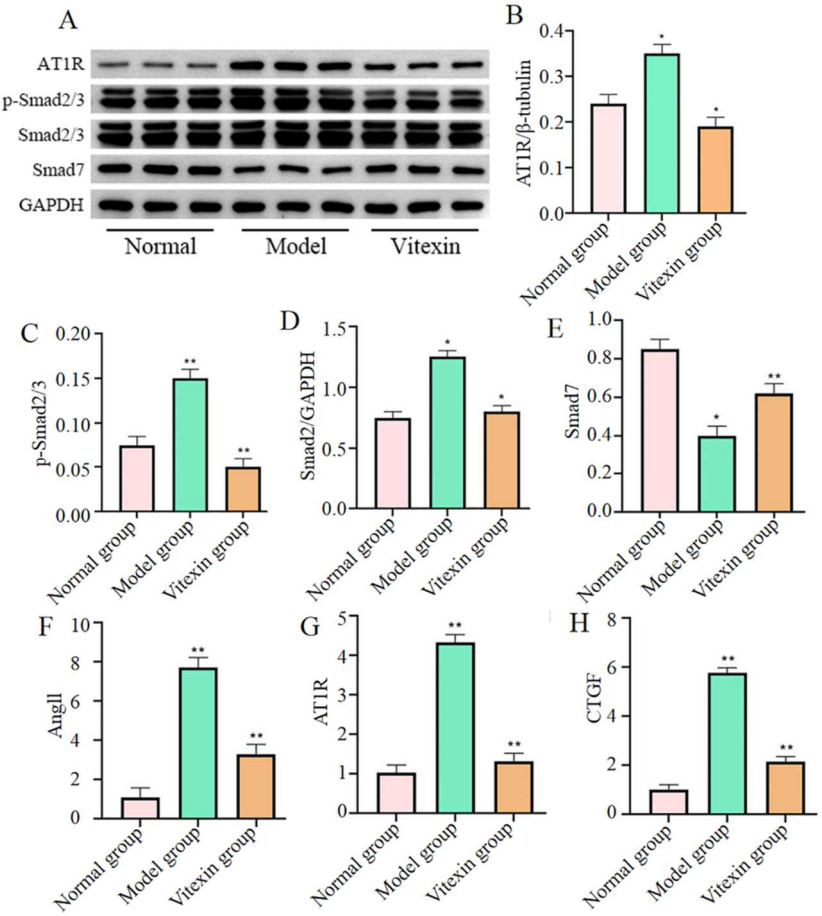

Fig. 7: The effect of Vitexin on the expression of AT1R, SMADs-related proteins and mRNA in renal tissues of mice with Ang II-induced renal injury.
(A): Protein expression bands of AT1R, p-Smad2/3, Smad2, Smad7, and GAPDH in kidney tissue of each group; (B): Relative expression level of AT1R; (C): Relative expression level of p-Smad2/3; (D): Relative expression level of Smad7; (E): Relative expression level of Smad2; (F): Relative expression level of AT1R mRNA; (G): Relative expression level of CTGF mRNA; (H): Relative expression level of Smad2 mRNA; *P < 0.05, **P < 0.01 compared with the model group. Data are expressed as mean ± SD (n=6).

It should be noted that although the observed changes in expression correlate with phenotypic improvement and align with the logic of known pathways, this study has not established the causal necessity of AT1R/Smad3 in Vitexin's effects, using methods such as genetic intervention or specific inhibitors. Therefore, these mechanistic inferences still require further validation via gain-of-function and loss-of-function experiments in subsequent studies.

A key strength of this study is that it is the first to systematically evaluate the impact of Vitexin on the AT1R/Smad3 pathway in an Ang II-induced renal injury model, with verification at both cellular and animal levels. However, this study also has several limitations. First, its scope is limited to preclinical exploration and does not cover key translational research aspects such as drug metabolism, toxicology, or formulation development. Second, although we endeavored to minimize selection bias, performance bias, and measurement bias through measures such as randomization, blinded assessment, and strict control of experimental conditions, and to identify and control for major confounding variables (e.g., solvent effects, individual animal differences), some potentially uncontrolled confounding factors remain. For instance, variables such as food intake and circadian activity rhythms, which may influence metabolism and blood pressure, were not monitored in the animal experiments. *In-vitro* studies did not examine the effects of cell density or medium batch variations on the response to Ang II.

Furthermore, *in vitro experiments used only HK-2 cells and did not include other key renal cell types,* such as mesangial cells or podocytes. The mechanistic investigation relied primarily on correlations in protein and mRNA expression, lacking functional validation experiments such as AT1R knockdown or Smad3 silencing. Consequently, a definitive causal pathway relationship cannot be established.

The results of this study indicate that Vitexin can ameliorate Ang II-induced decreases in HK-2 cell viability, alleviate renal tissue injury, glomerulosclerosis and fibrosis in mice. Its mechanism may be related to inhibiting the AT1R/Smad3 signaling pathway, upregulating Smad7 and downregulating CTGF expression. These findings provide experimental evidence supporting Vitexin as a potential intervention molecule for Ang II-related renal injury. However, its specific molecular targets, *in-vivo* pharmacodynamics and clinical applicability require further exploration.

Within the defined scope of this study and through a relatively rigorous experimental design (including bias control and management of confounding variables), the protective effect of Vitexin in an Ang II-induced renal injury model and its association with the AT1R/Smad3 pathway were confirmed. These findings provide preliminary evidence for considering Vitexin as a candidate natural molecule against renal fibrosis. Nonetheless, advancing it toward clinical application necessitates crossing a series of translational research stages, including, but not limited to: elucidating its *in-vivo* metabolic processes and active forms; conducting systematic safety pharmacology and long-term toxicity evaluations; optimizing drug delivery systems to enhance bioavailability and targeting; and ultimately, validation in more complex models that better approximate human disease (such as humanized models or non-human primate models).

CONCLUSION

In conclusion, vitexin ameliorates Ang II-induced reduction in HK-2 cell viability and alleviates renal tissue injury, glomerulosclerosis, and fibrosis in mice. The underlying mechanism may involve inhibition of the AT1R/Smad3 signaling pathway, upregulation of Smad7, and downregulation of CTGF expression. These findings provide experimental evidence supporting Vitexin as a potential intervention for Ang II-related renal injury. However, further exploration is required to elucidate its specific molecular targets, *in-vivo* pharmacodynamics and clinical applicability.

Acknowledgments
We gratefully acknowledge the Zhejiang Medical and Health Group Hangzhou Hospital for providing the necessary equipment for this study.

Authors' contributions
Yazhen Huang: Responsible for experimental design, performing major experiments, data collection and analysis and drafting the initial manuscript.
Wenshuai Mao: Participated in animal model establishment, *in-vivo* experimental data collection and statistical analysis.
Yalu Huang: Participated in cell experiments, molecular biological assays and partial data organization.
Hong Ge: As the corresponding author, was responsible for research conception, overall design, funding acquisition, project supervision, manuscript review and finalization.
All authors have read and approved the final manuscript.

Funding
There was no funding.

Data availability statement
The datasets generated during and/or analysed during the current study are available from the corresponding author on reasonable request.

Ethical approval
All animal experimental protocols in this study were approved by the Ethics Committee of Zhejiang Medical

and Health Group Hangzhou Hospital (Approval No.: SCXK(Zhe)2025-1201) and strictly adhered to international guidelines for the care of laboratory animals and the ARRIVE guidelines. This study was performed in adherence with the ARRIVE guidelines. See supplementary file for the ARRIVE checklist.

Conflicts of interest

All authors declare that there is no conflict of interest. This study did not receive any funding from commercial institutions or individuals that might affect the objectivity of the research.

Supplementary data

https://www.pjps.pk/uploads/2026/05/SUP1779524001.pdf

REFERENCES

Ahmad H, Khan H, Haque S, Ahmad S, Srivastava N and Khan A (2023). Angiotensin-converting enzyme and hypertension: A systemic analysis of various ace inhibitors, their side effects and bioactive peptides as a putative therapy for hypertension. *J Renin Angiotensin Aldosterone Syst*., **2023**: 7890188.

Cao Z, Wu Z, Duan T, Tang C, Huang D and Hu X (2022). Curcumin ameliorates HO-induced injury through SIRT1-PERK-CHOP pathway in pancreatic beta cells. Acta Biochim *Biophys Sin (Shanghai)*., **54**(3): 370-377.

Chen J, Chen C, Lv C, Feng R, Zhong W, Liu Y, Zhou S and Zhao M (2025). Vitexin enhances mitophagy and improves renal ischemia-reperfusion injury by regulating the p38/MAPK pathway. *Ren Fail*., **47**(1): 2463572.

Chen YQ, Zhou Y, Wang QL, Chen J, Chen H, Xie H H and Li L (2022). Conciliatory Anti-Allergic Decoction Attenuates Pyroptosis in RSV-Infected Asthmatic Mice and Lipopolysaccharide (LPS)-Induced 16HBE Cells by Inhibiting TLR3/NLRP3/NF-κB/IRF3 Signaling Pathway. *J Immunol Res*., **2022**: 1800401.

Cheng J, Jiang X, Deng Q, Ni L, Lin W, Cao W, Ren P, Xu B, Wang Q, Kuai J, Wu Y, Wei W and Wang C (2025). Inhibition of GRK2 mitigates renal fibrosis via oxidative stress pathway. *Eur J Pharmacol*., **1003**: 177887.

Dong X, Cao R, Li Q and Yin L (2022). The long noncoding RNA-H19 mediates the progression of fibrosis from acute kidney injury to chronic kidney disease by regulating the miR-196a/Wnt/β-catenin signaling. *Nephron*., **146**(2): 209–219.

Farooq A, Iqbal A, Rana NF, Fatima M, Maryam T, Batool F, Rehman Z, Menaa F, Azhar S, Nawaz A, Amin F, Mohammedsaleh ZM and Alrdahe SS (2022). A novel sprague-dawley rat model presents improved NASH/NAFLD symptoms with PEG coated vitexin liposomes. *Int J Mol Sci*., **23**(6): 3131.

Feng L, Chen C, Xiong X, Wang X, Li X, Kuang Q, Wei X, Gao L, Niu X, Li Q, Yang J, Li L and Luo P (2024). PS-MPs promotes the progression of inflammation and fibrosis in diabetic nephropathy through NLRP3/Caspase-1 and TGF-β1/Smad2/3 signaling pathways. *Ecotoxicol Environ Saf*., **273**: 116102.

Gregg LP, Richardson PA, Herrera MA, Akeroyd JM, Jafry SA, Gobbel GT, Wydermyer S, Arney J, Hung A, Matheny ME, Virani SS and Navaneethan SD (2023). Documented adverse drug reactions and discontinuation of angiotensin-converting enzyme inhibitors and angiotensin receptor blockers in chronic kidney disease. *Am J Nephrol*., **54**(3-4): 126–135.

Guo L and Shi L (2023). Vitexin improves cerebral ischemia-reperfusion injury by attenuating oxidative injury and ferroptosis via Keap1/Nrf2/HO-1signaling. *Neurochem Res*., **48**(3): 980–995.

Gisch DL, Brennan M, Lake BB, Basta J, Keller M S, Melo Ferreira R, Akilesh S, Ghag R, Lu C, Cheng Y H, Collins KS, Parikh SV, Rovin BH, Robbins L, Stout L, Conklin KY, Diep D, Zhang B, Knoten A, Barwinska D and Eadon MT (2024). The chromatin landscape of healthy and injured cell types in the human kidney. *Nat Commun*., **15**(1): 433.

Jiang YH, Guo JH, Wu S and Yang CH (2017). Vascular protective effects of aqueous extracts of Tribulus terrestris on hypertensive endothelial injury. *Chin J Nat Med*., **15**(8): 606–614.

Liu J, Chen Y, Zhang J, Zheng Y, An Y, Xia C, Chen Y, Huang S, Hou S and Deng D (2025). Vitexin alleviates MNNG-induced chronic atrophic gastritis via inhibiting NLRP3 inflammasome. *J Ethnopharmacol*., **340**: 119272.

Livak KJ and Schmittgen TD (2001). Analysis of relative gene expression data using real-time quantitative PCR and the 2(-Delta Delta C(T)) Method. *Methods.*, **25**(4): 402-408.

Livingston MJ, Shu S, Fan Y, Li Z, Jiao Q, Yin XM, Venkatachalam MA and Dong Z (2023). Tubular cells produce FGF2 via autophagy after acute kidney injury leading to fibroblast activation and renal fibrosis. *Autophagy*., **19**(1): 256–277.

Löptien J, Vesting S, Dobler S and Mohammadi S (2024). Evaluating the efficacy of protein quantification methods on membrane proteins. *Open Biol*., **14**(12): 240082.

Maji M, Acharya S, Bhattacharya I, Gupta A and Mukherjee A (2021). Effect of an imidazole-containing schiff base of an aromatic sulfonamide on the cytotoxic efficacy of N,N-coordinated half-sandwich ruthenium(II) p-cymene complexes. *Inorg Chem*., **60**(7): 4744–4754.

McKenney KM., Connacher RP, Dunshee EB and Goldstrohm AC (2024). Chemi-Northern: a versatile chemiluminescent northern blot method for analysis and quantitation of RNA molecules. *RNA*., **30**(4): 448-462.

Nasr AM, Moftah F, Abourehab MAS and Gad S (2022). Design, formulation and characterization of valsartan nanoethosomes for improving their bioavailability. *Pharmaceutics*., **14**(11): 2268.

Noor KK, Ijaz MU, Ehsan N, Tahir A, Yeni DK, Neamul

Kabir Zihad SM, Uddin SJ, Ashraf A and Simal-Gandara J (2022). Hepatoprotective role of vitexin against cadmium-induced liver damage in male rats: A biochemical, inflammatory, apoptotic and histopathological investigation. *Biomed Pharmacother*., **150**: 112934.

Rajabi S, Saberi S, Najafipour H, Askaripour M, Rajizadeh MA, Shahraki S and Kazeminia S (2024). Interaction of estradiol and renin-angiotensin system with microRNAs-21 and -29 in renal fibrosis: Focus on TGF-β/smad signaling pathway. *Mol Biol Rep*., **51**(1): 137.

Rojansky R, Sompuram SR, Gomulia E, Natkunam Y, Troxell M L and Fernandez-Pol S (2022). Digital Image Analysis and Quantitative Bead Standards in Root Cause Analysis of Immunohistochemical Staining Variability: A Real-world Example. *Appl Immunohistochem Mol Morphol*., **30**(7): 477-485.

Su Y, Shi D, Xia G, Liu Y, Xu L, Dao L, Lu X, Shen C and Xu C (2024). Carbonic anhydrase 3 is required for cardiac repair post myocardial infarction via Smad7-Smad2/3 signaling pathway. *Int J Biol Sci*., **20**(5): 1796–1814.

Wang L, Xu X, Zhang M, Hu C, Zhang X, Li C, Nie S, Huang Z, Zhao Z, Hou FF and Zhou M (2023). Prevalence of chronic kidney disease in China: Results from the sixth china chronic disease and risk factor surveillance. *JAMA Intern Med*., **183**(4): 298–310.

Wang Y, You YK, Guo J, Wang J, Shao B, Li H, Meng X, Lan HY and Chen H (2025). C-reactive protein promotes diabetic kidney disease via Smad3-mediated NLRP3 inflammasome activation. *Mol Ther*., **33**(1): 263–278.

Wu W, Wang X, Yu X and Lan HY (2022). Smad3 signatures in renal inflammation and fibrosis. *Int J Biol Sci*., **18**(7): 2795–2806.

Xu Z, Luo W, Chen L, Zhuang Z, Yang D, Qian J, Khan ZA, Guan X, Wang Y, Li X and Liang G (2022). Ang II (Angiotensin II)-Induced FGFR1 (Fibroblast Growth Factor Receptor 1) activation in tubular epithelial cells promotes hypertensive kidney fibrosis and injury. *Hypertension*., **79**(9): 2028–2041.

Ying M, Shao X, Qin H, Yin P, Lin Y, Wu J, Ren J and Zheng Y (2024). Disease burden and epidemiological trends of chronic kidney disease at the global, Regional, National Levels from 1990 to 2019. *Nephron*., **148**(2): 113–123.

Ye S, Huang H, Xiao Y, Han X, Shi F, Luo W, Chen J, Ye Y, Zhao X, Huang W, Wang Y, Lai D, Liang G and Fu G (2023). Macrophage dectin-1 mediates Ang II renal injury through neutrophil migration and TGF-β1 secretion. *Cell Mol Life Sci*., **80**(7): 184.

Zeng W, Wang T, Stürmer T, He N, Shen P, Lin H, Guan X and Xu Y (2025). Comparative effectiveness of angiotensin-converting enzyme inhibitors and angiotensin II receptor blockers on cardiovascular outcomes in older adults with type 2 diabetes mellitus: A target trial emulation study. *Cardiovasc Diabetol*., **24**(1): 194.

Zhu B, Ni Y, Gong Y, Kang X, Guo H, Liu X, Li J and Wang L (2023). Formononetin ameliorates ferroptosis-associated fibrosis in renal tubular epithelial cells and in mice with chronic kidney disease by suppressing the Smad3/ATF3/SLC7A11 signaling. *Life Sci*., **315**: 121331.

Zhou P, Zheng ZH, Wan T, Wu J, Liao CW and Sun XJ (2022). Erratum: Vitexin inhibits gastric cancer growth and metastasis through HMGB1-mediated inactivation of the PI3K/AKT/mTOR/HIF-1α signaling pathway. *J Gastric Cancer*., **22**(2): 156.

Zhao K, Zhu H, He X, Du P, Liang T, Sun Y, Jing Z and Zhou J (2023). Senkyunolide I ameliorates thoracic aortic aneurysm and dissection in mice via inhibiting the oxidative stress and apoptosis of endothelial cells. *Biochim Biophys Acta Mol Basis Dis*., **1869**(7): 166819.